



Feasibility analysis of synthesized polyaniline nanocomposites loaded by Co-doped ZnO nanorods for aqueous pollutants oxidation

Belal A. Tahoun^{1,2} · Elsayed M. Farag² · Maha A. Tony^{1,2} · Shehab A. Mansour^{1,2}

Received: 4 April 2022 / Accepted: 9 October 2023 / Published online: 4 November 2023
© The Author(s) 2023

Abstract

Polyaniline (PANI) nanocomposites (NCs) based on cobalt (Co)-doped ZnO nanorods were fabricated (PANI-NCs) using chemical oxidation polymerization technique. Co-doped ZnO nanorods were synthesized using hydrothermal route. Microstructure characterization and UV–Visible absorption measurement confirm the formation of wurtzite ZnO nanostructured crystals. Introducing effect of Co-doped ZnO nanorods into PANI matrix on microstructural, optical, surface morphology and electrical properties of the investigated NCs were studied. The characterization of the fabricated NCs was examined using X-ray diffraction (XRD), Fourier transform infrared (FTIR), high-resolution transmission electron microscopy (HR-TEM) and four-probe DC electrical conductivity. Also, the photocatalytic activity of the fabricated NCs was examined using UV irradiation for Procion Blue dye wastewater oxidation. The photocatalytic experimental parameters were studied and the results revealed high photocatalytic activity reached to complete dye removal within 60 min of irradiation time (at pH 7.0 and room temperature). Finally, the data fitted with first-order kinetic model.

Keywords Photocatalysis · Wastewater · Semiconductors · Conducting polymers · Reaction kinetics

Introduction

Zinc oxide (ZnO) is a wide band-gap II–VI semiconductor, low cost and low toxicity that has attracted resurgent interest for numerous applications. It attracted the researchers' interest for their exceptional optical, luminescent, electronic, optoelectronic and photocatalytic properties (Ocakoglu et al. 2015; Mansour et al. 2017). Also, ZnO nanocrystals show novel physical and chemical properties in comparison with their bulk forms (Mansour et al. 2017). Recently, several methods were used to synthesize ZnO nanocrystals in one-dimensional (1D) structures with various morphologies such as nanowires, nanorods, nanoneedles and nanorings (Ocakoglu et al. 2015; Cia et al. 2023; Liu et al. 2023). The

distinctive properties resulting from the distinctive morphologies would open up new opportunities for ZnO nanomaterials to be qualified for several functional devices (Ocakoglu et al. 2015; Ozgür et al. 2005). The use of ZnO nanostructured material as a photocatalyst for removal of organic pollutants is considered one of the promised applications of such material. Although of that, pristine ZnO usually shows some limitations in field of photocatalysis due to the high probability of the recombination process between photoinduced electrons and holes. So, there are lot of research works that have been introduced to enhance the separation rate of the photoinduced charge carriers doping the pristine ZnO with metallic ions (Yu et al. 2002). The doping with small amount of such metallic ions could be enabled to adjust the electronic energy band structure by increasing density of trap levels with keeping the original vital properties of the photocatalysts (Wang et al. 2023). Cobalt (Co)-doped ZnO is considered one of the most important ZnO-based compounds for the abundant electron states of Co and similarity between Co ionic radius and that of Zn which increase the solubility of Co in ZnO matrix (Farha et al. 2016; Chen et al. 2023). In view of the benefits and limitations of such photocatalytic materials, there are attempted to optimize their photocatalytic activity by various methods. In this respect,

✉ Maha A. Tony
dr.maha.tony@gmail.com

¹ Advanced Materials/Solar Energy and Environmental Sustainability (AMSEES) Laboratory, Faculty of Engineering, Menoufia University, Shebin El-Kom 32511, Egypt

² Basic Engineering Science Department, Faculty of Engineering, Menoufia University, Shebin El-Kom 32511, Egypt

altered strategies were used, such as surface and interface adjustment by controlling morphology, particle size, composite or coupling materials such as conducting polymers (CPs), transition-metal doping, nonmetal doping, co-doping with different configurations, noble-metal deposition and surface sensitization by organic dye and metal complexes, to improve the photocatalytic feature. Recently, conductive polymers such as polyaniline (PANI) has much interest in the photocatalysis applications due to its remarkable chemical stability compared to other CPs, facile synthetic route, relatively high electrical conductivity and high ability of dispersion. The coupling of PANI with various semiconductor materials, such as ZnO, CoFe_2O_4 , TiO_2 and Bi_3NbO_7 , has been reported for enhancing the photocatalytic activity (Sharma et al. 2016).

Worldwide, synthetic dyes are produced and used in numerous industrial applications, such as textile, leather tanning, food processing, cosmetics, electroplating, paper and pharmaceutical industries; otherwise, about 5–10% of such dyes are released into the ecosystem (Epolito et al. 2005; Yahya et al. 2008; Bazin et al. 2012). However, those dyes possess a hazard effect to the environment since they significantly compromise the aesthetic quality of water bodies, increase biological and chemical oxygen demand (BOD and COD), impair photosynthesis, inhibit plant growth, enter the food chain and may promote toxicity and cause carcinogenic effects to the human bodies (Lellis et al. 2019). Hence, treating and mineralizing such dyes from wastewater streams is a must. Various conventional chemical or may be biological treatment technologies are introduced to eliminate dyes from aqueous effluents. But, those conventional technologies are unfavorable since their high treatment cost or they may be transferred the pollutants from one phase to another without mineralizing them (Thabet et al. 2021). To add up, a concentrated sludge is resulting from treatment that requires further treatment. Also, such techniques could not reach to complete pollutants elimination from wastewater. Moreover, those methodologies are insufficient in removing small concentrations nor low reaction rates (Tony et al. 2018). Photocatalytic oxidation technology, is signified as one AOT, has been emerged as superior efficient reactions (Tony 2020). Photocatalytic oxidation is based on the formation of high reactive groups, such as $\cdot\text{OH}$ radicals, which are responsible of oxidizing and mineralizing such pollutants to harmless end products, such as CO_2 , H_2O and inorganic matter (Tony and Mansour 2019). Several catalysts have been introduced as a source of catalytic oxidants, i.e., ZnO (Tony and Mansour 2020a, b, c), TiO_2 (Kositzi et al. 2004; Tony and Mansour 2020a) and iron oxides (Pirsaheb et al. 2019; Tony and Ali 2022), are subjected as photocatalyst for wastewater oxidation. However, searching for novel coupled materials with sufficient treatment capabilities and innovative characteristics is attaining the scientists' attention. In this respect, PANI/

ZnO and PANI/AL-doped ZnO have been emerged quite good results through their usage in AOT under visible light as reported in degradation of methylene blue and methylene orange, respectively (Mitra et al. 2017; Olad and Nosrati 2012). The present work aims to study some physical properties for PANI nanocomposites loaded by Co-doped ZnO nanorods to investigate the photocatalytic performance of such nanocomposites. The usage of Co as doping element to ZnO matrix could be enabled from the shift of the optical absorption edge toward visible-light region that is leading to narrowing in band-gap energy. So, doping of ZnO with Co extends the absorbing region to the Vis spectrum (Murakrishna and Manickam 2017). Moreover, the Co-doped ZnO nanorods as 1D nanostructured material offered good interaction with PANI matrix, especially with high aspect ratio of the investigated nanorods. Accordingly, the PANI nanocomposites loaded by Co-doped ZnO nanorods is considered a novel and a promise catalyst. The fabricated PANI/ Co-doped ZnO nanocomposites are introduced to be a photocatalyst to oxidize Procion Blue dye wastewater effluent which simulated the textile stream aqueous discharge.

Materials and methods

Materials

The used reagents in the hydrothermal synthesization and the polymerization processes were of analytical grade and no further purification was done. Zinc acetate dihydrate ($\text{Zn}(\text{CH}_3\text{COO})_2 \cdot 2\text{H}_2\text{O}$; Winlab), cobalt acetate hydrate ($\text{Co}(\text{CH}_3\text{COO})_2 \cdot 4\text{H}_2\text{O}$, Aldrich), sodium hydroxide (NaOH, ADWIC) and ethanol (Aldrich) were used in synthesization of Co-doped ZnO nanorods. However, aniline provided from Aldrich, ammonium persulfate (APS, bioWORLD) and hydrochloric acid (HCL 37%, spectrum) were utilized in PANI polymerization process.

Synthesization of Co-doped ZnO nanorods

Co-doped ZnO nanorods were synthesized via hydrothermal route as seen in Fig. 1a. In the typical route, Co and Zn precursors were dissolved in ethanol at room temperature (RT) to form 0.1 M solution. The used molar percentage of $\text{Co}(\text{NO}_3)_2 \cdot 6\text{H}_2\text{O}$ is 0, 1, 3, 5 and 7% from the total concentration of precursors. Separately a solution of 0.5 M from NaOH in ethanol was prepared. For each sample, 10 mL of Co and Zn precursors was gradually added to 20 mL of NaOH solution under stirring to get clear solution. Then, the obtained clear solution was introduced to Teflon-lined stainless-steel autoclave and heated at 140 °C for 24 h. After slow cooling, the precipitate was collected and washed with water and ethanol for three times using Whatman filter paper. The

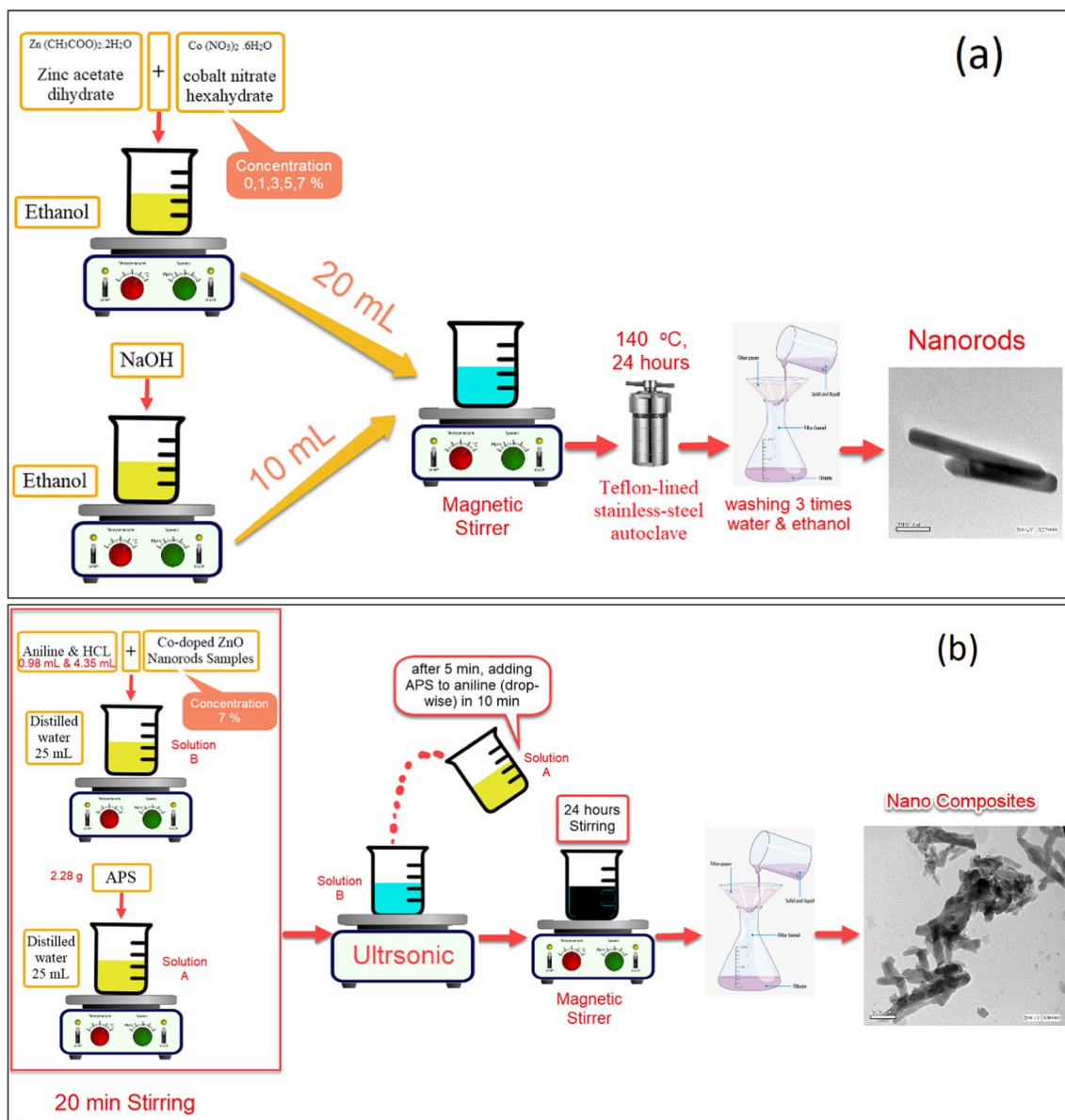


Fig. 1 Schematic diagram for **a** hydrothermal process of synthetization of Co-doped ZnO nanorods, **b** PANI nanocomposites polymerization process in the presence of Co-doped ZnO nanorods

collected precipitate was dried in air at RT for 48 h. The obtained sample powders are fine with color varied from moderate green to light green for the doped samples with the decrease in Co concentration, whereas the pristine ZnO sample is in off-white color. The Co-doped ZnO nanorod samples are labeled as CZ0, CZ1, CZ3, CZ5 and CZ7, corresponding to the utilized molarity concentration of $Co(NO_3)_2 \cdot 0.6H_2O$; 0, 3, 5 and 7%, respectively.

Fabrication of PANI/Co-doped ZnO nanocomposites

PANI/Co-doped ZnO nanocomposites were fabricated using the direct oxidation of aniline in acidic solution as

seen in Fig. 1b. The acidic for all composites are constant by using the same amount of HCL. The weight ratio of Co-doped ZnO nanorods to aniline was 7:93%, accordingly the obtained nanocomposites labeled as PANI-CZ0, PANI-CZ1, PANI-CZ3, PANI-CZ5 and PANI-CZ7. The used full weight of nanorods and aniline was 1 g. The oxidant aqueous solution was prepared by dissolving 2.28 g from APS in 25 mL of distilled water. Separately, the desired amount of aniline and the synthesized nanorod samples was added from previously prepared acidic solution using 25 mL distilled water and 4.35 mL HCL. After 20 min of stirring, the aniline-nanorods solution was sonicated for 5 min to get good dispersion of nanorods in the solution. Thereafter, the prepared

oxidant solution was added in a drop-wise fashion into the aniline-nanorods solution during ~ 10 min under exposing to sonication. The gotten solution kept under stirring for one day at RT to complete the process of polymerization. The nanocomposites were obtained from the suspended solution by filtration and washing three times with distilled water and ethanol. Finally, PANI/ Co-doped ZnO nanocomposites were dried vacuum overnight at 50 °C.

Characterizations and measurements

The phase structure of the synthesized Co-doped ZnO nanorods as well as the fabricated PANI nanocomposites was obtained by using XRPhillips X'pert-MPD3040 diffractometer using monochromatic CuK- α with 1.5406 Å wavelength. The step-scan mode was used to register the intensities of the diffracted X-rays with 0.02° step over 2θ ranging from 10° to 80°. The morphology of both synthesized Co-doped ZnO nanorods and the investigated PANI/NC nanocomposites were examined via JEM-2100 high-resolution transmission electron microscope (HR-TEM). The Fourier transform infrared (FTIR) measurements of the synthesized nanorods and nanocomposites were recorded in the wavenumber ranging from 400 to 4000 cm^{-1} via JASCO FT/IR-4100 spectrometer. The UV–Vis absorption spectra throughout the wavelength range of 200–800 nm for the alcoholic diluted solutions of the synthesized Co-doped ZnO samples were obtained by using UV–Vis spectrophotometer of type Unico UV-2100 that is to measure in scan mode via step motor to scan the wavelength range with step 1 nm.

For DC measurements, the fabricated PANI/ Co-doped ZnO NCs were pressed under five tons to form pellet samples in the shape of disk with diameter equal to 1 cm and thickness around 0.15 cm and. The DC conductivity (σ) of the nanocomposite samples was measured using four-probe method and carried out using KEITHLEY 2635A System SourceMeter. A LabVIEW-based software was utilized in transferring and controlling the obtained data from the sourcemeter using IEEE-488-GPIB. The value of σ was determined by the reciprocal of the resistivity (ρ) which recorded via the used LabVIEW. The values of ρ were obtained from the linear slope of current (I)–voltage (V) plot, where the used values of I and V are the average of that collected for 16 times at each measuring step. The value of ρ was calculated using the following equation (Schroder and Corporation 2006):

$$\rho = 2\pi SF \frac{V}{I} \quad (1)$$

where S is the probe spacing, here is 0.2 cm, and F is correction factor depending on the sample dimension and probe placement (Schroder and Corporation 2006).

Photo-oxidation experiments

To evaluate the photocatalytic activity of the all-synthesized samples, Co-doped/PANI, on Procion Blue MX-7RX dye oxidation, a simple photochemical reactor is used which consists of ultraviolet illumination source using UV lamp (model UV-12 W, 230 V and 50 Hz with 253.7 nm wavelength) enclosed in silica glass jacket immersed in a glass container. The dye solution is subjected to the glass container after the pH is adjusted, if required (Adwa AD1030 pH/mV and temperature meter, thereafter the prepared photocatalyst at certain doses is added to initiate the reaction). The solution is subjected to a magnetic stirring to ensure mixing and dispersion. Then, samples were withdrawn periodically for spectrophotometric analysis at a maximum wavelength of 570 nm using Unico UV-2100 Spectrometer. The schematic representation of the experimental setup is given in Fig. 2.

Results and discussion

Structure and morphological characterization of Co:ZnO nanostructured samples

Figure 3 displays XRD patterns of the synthesized Co:ZnO samples. The XRD patterns of all the investigated samples reveal the formation of a wurtzite ZnO structure, in agreement with standard JCPDS Card: 36-1451 (Cheng and Samulski 2004). Moreover, there are any other peaks assigned to other ZnO phases and/or phases for Co and cobalt oxides.

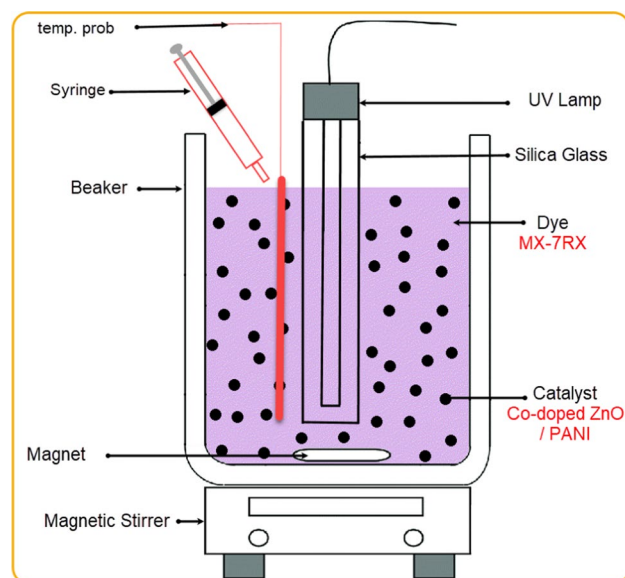


Fig. 2 Schematic representation of the experimental setup of the photocatalytic experiment

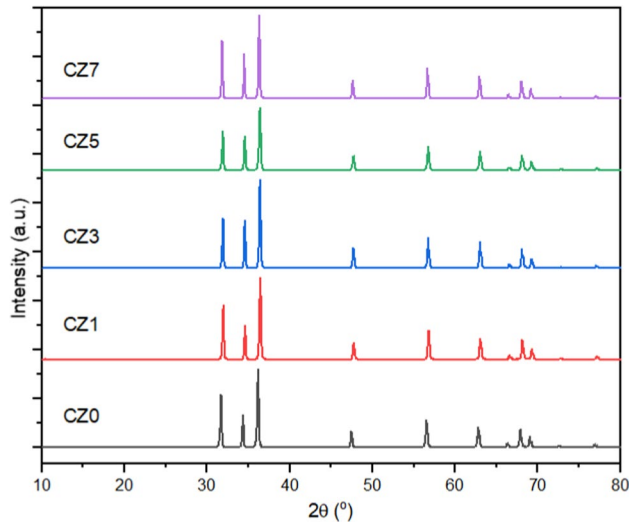


Fig. 3 The XRD patterns of a ZnO and Co-doped ZnO nanorods

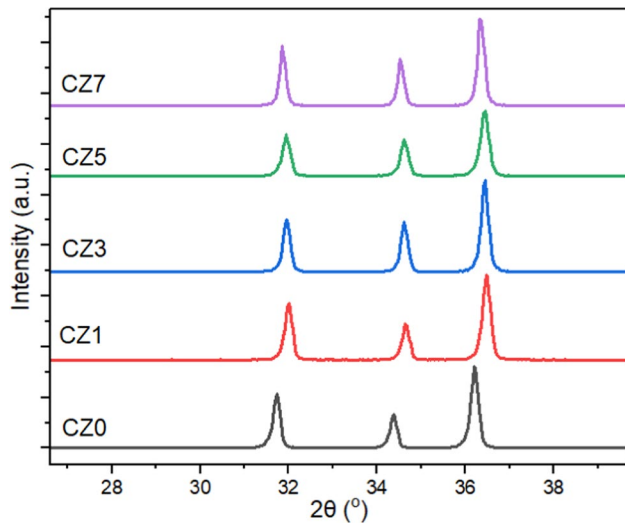


Fig. 4 The XRD patterns of a ZnO and Co-doped ZnO nanorods (1st three peaks)

Such result about the absence of other additional phases has been reported in many research works for Co:ZnO samples using various preparation techniques even with high concentration of Co, see, for example, (Farha et al. 2016; Mesaros et al. 2014a; Hammad et al. 2013; Kumbhakar et al. 2008;

Kaphle et al. 2019). The formation of only single-phase structure, wurtzite ZnO, has been attributed to substitution of Co ions in zinc sites in the lattices of ZnO (Farha et al. 2016). Moreover, Fig. 4 shows the shift in the positions of the first three diffraction peaks of the investigated Co:ZnO samples to higher 2θ values with increasing in Co contents. This shift is commonly obtained for Co-doped ZnO compositions and confirming to the occupation of Co ions at the Zn sites in the host structure (Ozgür et al. 2005; Farha et al. 2016; Shi et al. 2013).

The crystalline size (D) of Co:ZnO samples could be estimated using the value of full-width at half maximum (FWHM) for the obtained diffraction peaks according the following Debye–Scherrer relation (Scherrer 1918; Patterson 1939; Langford and Wilson 1978).

$$D = \frac{0.9\lambda}{\beta \cos\theta} \tag{2}$$

where λ , β and θ are the wavelength of the used X-ray, FWHM and the Bragg diffraction angle, respectively. The calculated values of D via Eq. 2 for all the investigated Co:ZnO samples showed the nanostructure formation using all the recorded diffraction lines of each sample, where the obtained D values are between 32.4 and 39 nm as illustrated in Table 1 with mean value of 35.8 ± 2.8 nm, while the values of D for each sample using the most preferred orientation at (101), D_{101} , are between 34.1 and 42.7 nm with mean value of 38.2 ± 3.1 nm. Although the Debye–Scherrer method is a well-known method that uses XRD patterns to calculate the crystallite size based on FWHM of the diffraction peak, it neglects the peak the probable broadening that obtained from the inhomogeneous strain and instrumental effects (Varghese and Pradeep 2003). Accordingly, Williamson–Hall (W–H) plot could be used to provide information about lattice strain, ϵ , and effective particle size, D_{W-H} , for the investigated samples. The W–H equation has the following form (Williamson and Hall 1953):

$$\frac{\beta \cos\theta}{\lambda} = \frac{1}{D_{W-H}} + \frac{\epsilon \sin\theta}{\lambda} \tag{3}$$

Figure 5 represents the plot between $\frac{\beta \cos\theta}{\lambda}$ versus $\frac{\sin\theta}{\lambda}$. As shown in Fig. 5, the obtained linear relation has a positive slope for all the investigated nanoparticles which ascribed

Table 1 Particle size and lattice parameter of Co-doped ZnO samples

Sample	D (nm)	D_{101} (nm)	D_{W-H}	$\epsilon \times 10^{-3}$	a (Å)	c (Å)	ca	V (Å ³)
CZ0	36.2	38.5	72.78	4.75	3.254	5.215	1.603	47.793
CZ1	35.2	36.8	61.01	3.88	3.224	5.171	1.604	46.531
CZ3	36.2	38.9	77.76	5.15	3.228	5.177	1.603	46.713
CZ5	32.4	34.1	54.64	4.05	3.232	5.177	1.602	46.815
CZ7	39	42.7	97.85	5.49	3.237	5.194	1.605	47.109

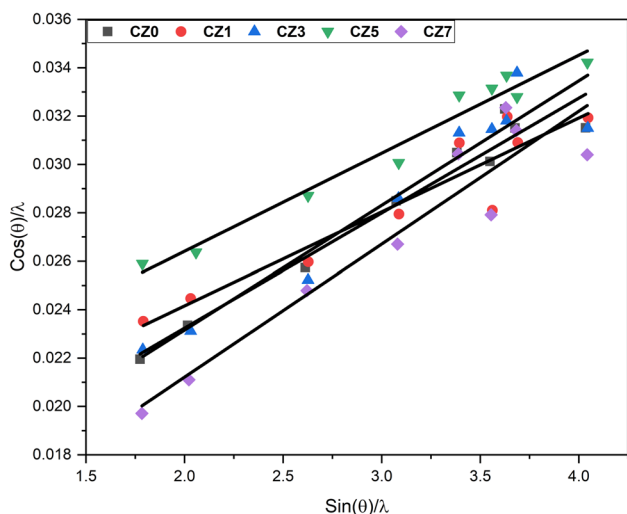


Fig. 5 Williamson–Hall plot of Co-doped ZnO nanorods

to tensile strain in crystals of the studied Co:ZnO samples (Senthilkumar et al. 2010). The calculated values of the tensile strain and the effective particle size are listed in Table 1.

Lattice constants (c and a) for the wurtzite ZnO structure and their ratio were estimated from the XRD data for investigated Co:ZnO nanoparticle samples using the relation; $\frac{1}{d_{hkl}^2} = \frac{4}{3} \left(\frac{h^2+k^2+hk}{a^2} \right) + \frac{l^2}{c^2}$ (Chatterjee 2008). The obtained lattice constant and the volume of unit cell of the studied nanoparticles are listed in Table 1. The calculated values of a and c of Co-doped ZnO samples are very close to these obtained

for pure ZnO sample that confirms the substitution of Zn ions by Co ions without great change in the volume of the unit cell (Farha et al. 2016; Neto et al. 2019; Nirmala and Anukaliani 2011). Figure 6 shows comparison between particle size obtained from Scherrer, average particle size of all peaks, and Williamson–Hall methods. The variation in both methods takes approximately the same trend.

The HR-TEM micrographs in Fig. 7 reveal that the Co-doped ZnO in nanorods shape with reasonable uniformity in size. 1D nanostructure shape is expected for ZnO nanocrystals that is synthesized using hydrothermal route. The obtained micrographs for all the investigated samples showed agglomerated features of the nanorods. In fact, the nanoparticles be likely to agglomerate together due to their highly surface energy, intrinsic crystal structure and external factors such as temperature, solvents and impurities (Cheng and Samulski 2004). Moreover, the investigated Co–ZnO samples displayed commonly magnetic feature for their room temperature ferromagnetic behavior (Mansour et al. 2021).

UV–Visible absorbance spectroscopy of Co:ZnO nanostructured samples

The UV–Visible absorption measurements were done by dispersing the synthesized nanoparticles in ethanol with 1 mg/mL concentration for each studied Co:ZnO sample. Figure 8 presents the UV–Visible absorption spectra of the pristine and Co-doped ZnO samples with various

Fig. 6 Comparison between the particle size calculated by Scherrer and Williamson–Hall (W–H) methods

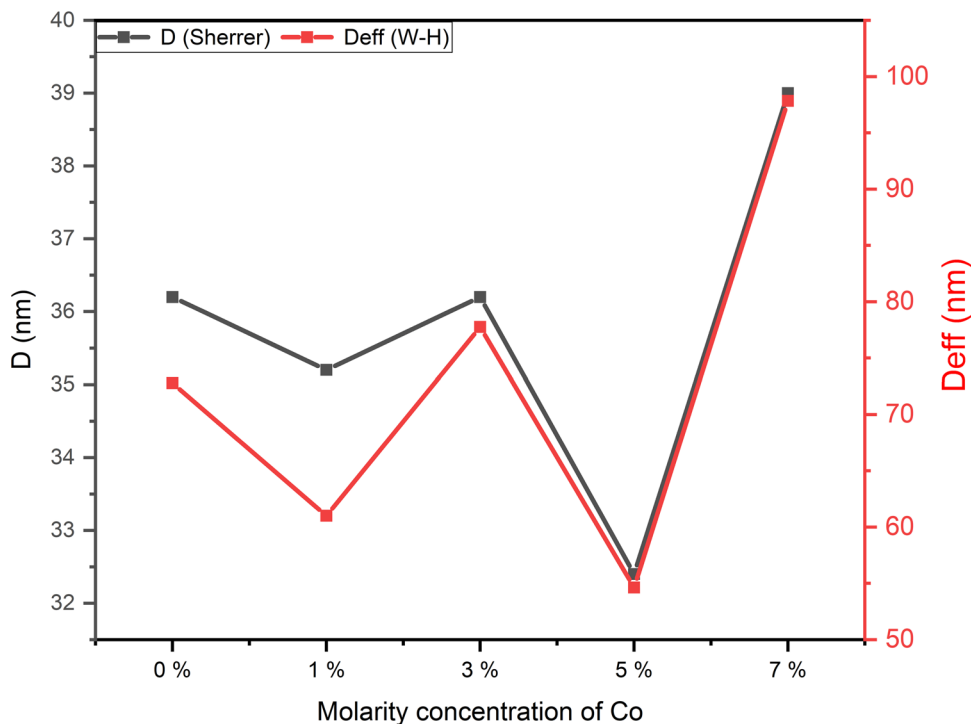
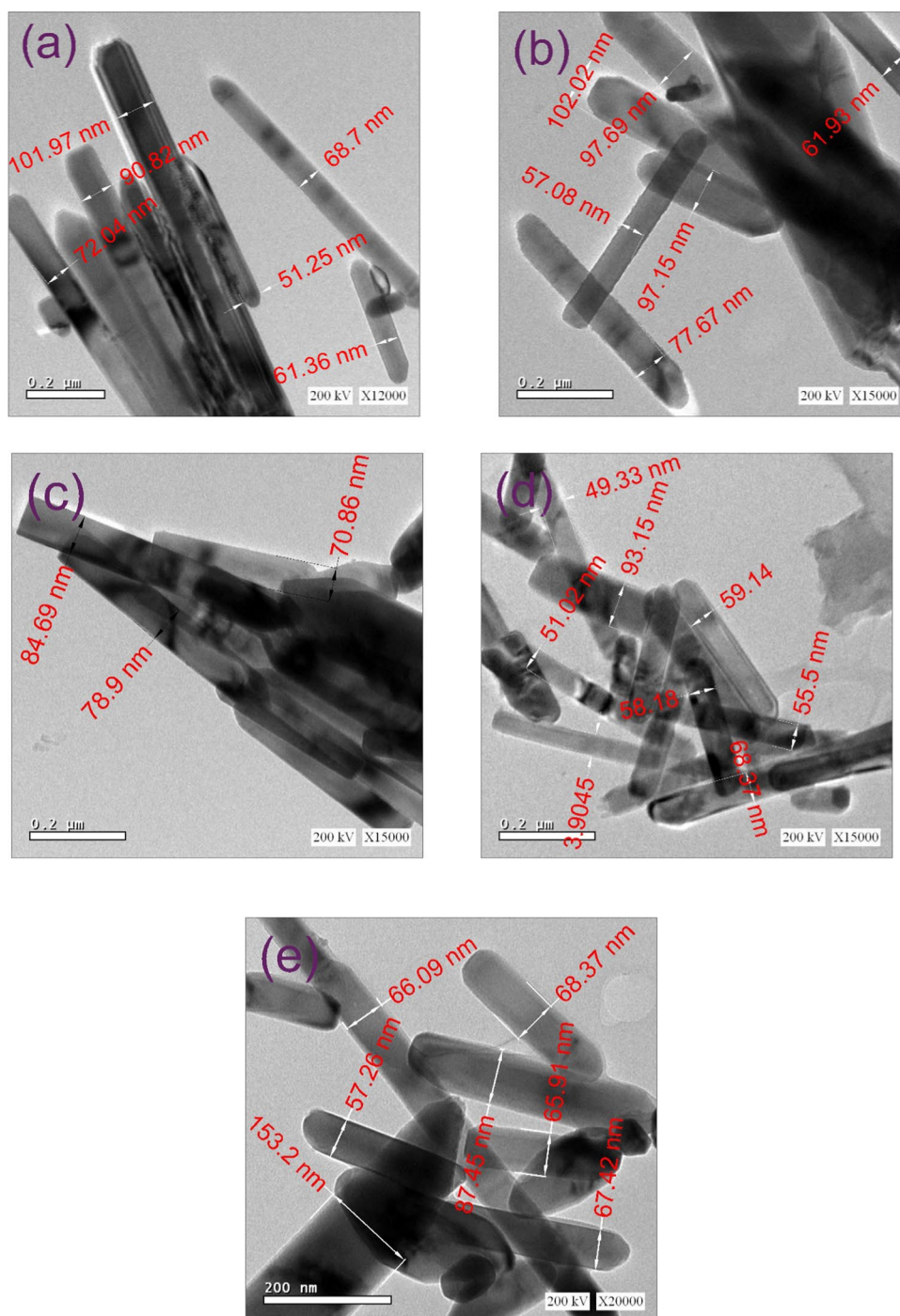


Fig. 7 HR-TEM micrographs of Co-doped ZnO samples; CZ0 (a), CZ1 (b), CZ3 (c), CZ5 (d), CZ7 (e)



concentrations of Co. Such figure revealed strong well-defined absorbance peak for all the investigated samples at close range from 374 to 362 nm and the peak values showed blue shift with increase in the Co concentration. This shift could be attributed to *sp-d* exchange interactions between the localized 3d electrons of Co^{+2} ions and *sp* band electrons of the host ZnO nanocrystals (Nirmala and Anukaliani 2011; Hammad et al. 2012). Due to this interaction, the Fermi level merges into the conduction band

with an increase in the carrier concentration. Thus, the low energy transitions are blocked. The obtained results are in good agreement with the results reported by Sakai et al. (2006). The insertion of the cobalt Co ions into the ZnO structure leads to the appearance of an additional absorption peak (Mesaros et al. 2014b) at around 408 nm for all the doped samples.

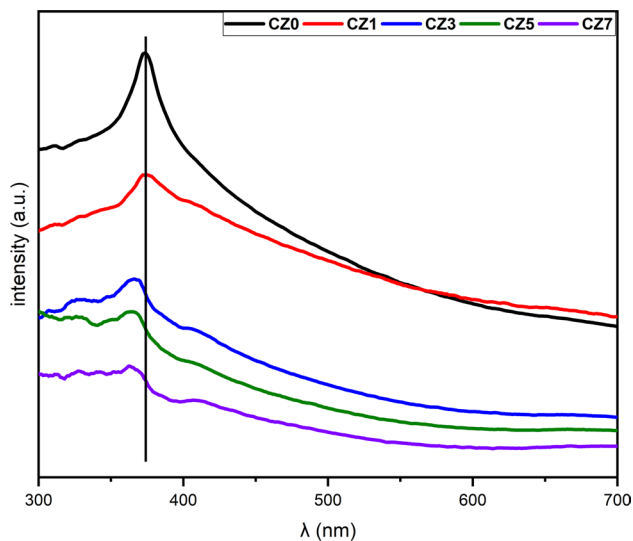


Fig. 8 UV-Vis spectra of pure and Co-doped ZnO nanorods

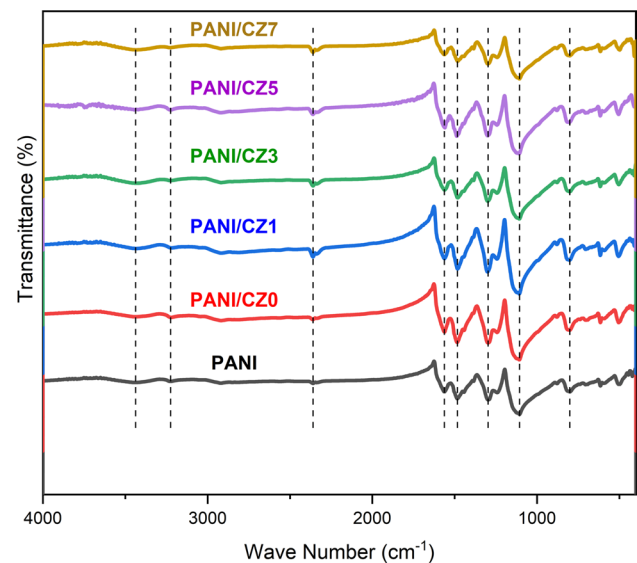


Fig. 10 FTIR for PANI/Co-doped ZnO nanocomposites

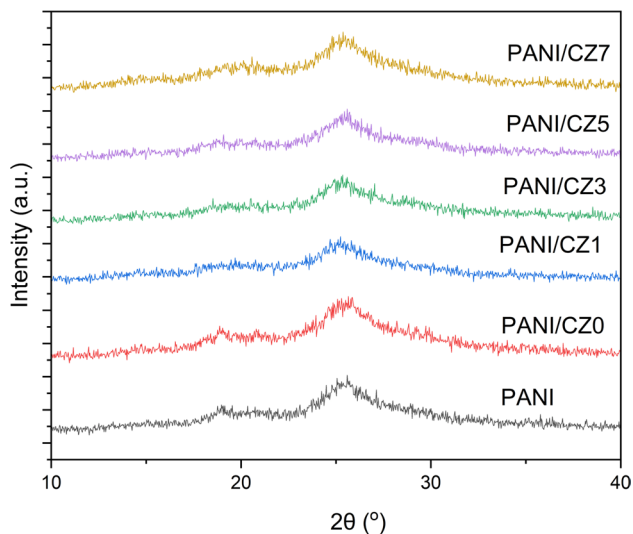


Fig. 9 XRD patterns of PANI/Co-doped ZnO nanocomposites

Structure and morphological characterization of the fabricated PANI/Co-doped ZnO nanocomposites

Figure 9 shows the obtained XRD patterns of PANI/Co-doped ZnO nanocomposites. The obtained diffraction peaks for pure PANI sample at $2\theta = 15.2^\circ$, 20.5° and 25.2° with a d spacing of 5.8 Å, 4.3 Å and 3.5 Å, respectively, which shows low crystallinity of the CPs due to repetition benzenoid and quinoid rings in PANI chains (Shi et al. 2009). The recorded diffraction peaks for all the investigated nanocomposites confirm the formation of PANI with such diffraction angle range due to the parallel and perpendicular periodicity of the

Table 2 Characteristic peaks obtained from FTIR spectrum of PANI/Co-doped ZnO nanocomposites

#	Wave number (cm ⁻¹)	Peak related bond
1	800.95	C–H stretching mode of the PANI benzenoid ring
2	1106.47	C–H bonding
3	1296.97	C–N stretching mode of the benzenoid rings
4	1483.93	C–C stretching of benzenoid rings
5	1562.72	C=C stretching of quinoid ring
6	2359.33	C=O bonding
7	3224.78	N–H stretching vibration
8	3437.94	N–H stretching vibration of amine group

PANI chains (Mostafaei and Zolriasatein 2012). The peak at $2\theta = 25.2^\circ$ is stronger than that obtained at $2\theta = 20.5^\circ$, the same results usually obtained for highly doped emeraldine PANI (Pouget et al. 1991; Xia and Wang 2002). Such results suggest the successful high doping level of the synthesized PANI nanocomposites.

FTIR analyses were carried out to investigate the chemical functional interaction of Co-doped ZnO nanoparticles with the PANI matrix. In this respect, Fig. 10 shows the FTIR spectra of PANI/Co-doped ZnO nanocomposites. As can be seen from Fig. 10, the absorption peaks at 615, 801, 1106, 1297, 1484, 1563, 2359 and 3213 cm⁻¹ are consequent to the characteristic absorption and vibration modes of PANI (Mansour et al. 2021). Table 2 briefly describes the peaks and their corresponding bonds. The absorption peaks at 1563 cm⁻¹ and around to 1484 cm⁻¹ which correspond to quinone- and benzene-ring stretching

vibrations, respectively, showed slight shift to higher values of wavenumbers that is referring to strong interaction between PANI and Co-doped ZnO nanoparticles (Zamani et al. 2019). The same trend was obtained for the absorption peak at 1106 cm^{-1} that is assigned to the aromatic C–H in-plane bending modes.

Figure 11 shows the HR-TEM micrographs of PANI/CZ1 and PANI/CZ5 nanocomposites. The gotten PANI polymer shows ribbon-like nanofiber shapes, as manifested by white arrows, with high degree of agglomerations especially for PANI/CZ1 sample. Moreover, Fig. 11 shows the combination between PANI and Co-doped ZnO nanoparticles. Figure 11 shows the combination between PANI and the Co-doped ZnO nanorods (as manifested by black arrows) which refers to that the quite dispersion of the Co-doped ZnO nanorods in the polymer matrix due to ultrasonic radiation in situ of polymerization process of aniline. The PANI ribbon-like structure eased the dispersion of

the Co-doped ZnO nanorods in the polymer matrix that confirms the interaction between PANI and the nanorods.

DC Electrical conductivity of the fabricated PANI/Co-doped ZnO nanocomposites

Figure 12 shows the obtained values of σ at RT for PANI/Co-doped ZnO nanocomposites using the four-point probe measurement technique. Each obtained value of conductivity (σ) represents the average of measurements for three times. The obtained values of σ for the investigated samples are close to each other with nonmonotonic trend. Such result could be attributed to the usage of the same weight percentage of Co:ZnO nanoparticles. Although of that, the highest values of σ are obtained for PANI/CZ1 sample and are found to be $3.918 \times 10^{-5}\ \Omega^{-1}\text{ cm}^{-1}$. The nonmonotonic trend of σ with Co/Zn molarity ratio could be attributed to the features of the filler such as size, shape and agglomeration (Cho et al. 2001). Here, one can notice that, the used filler,

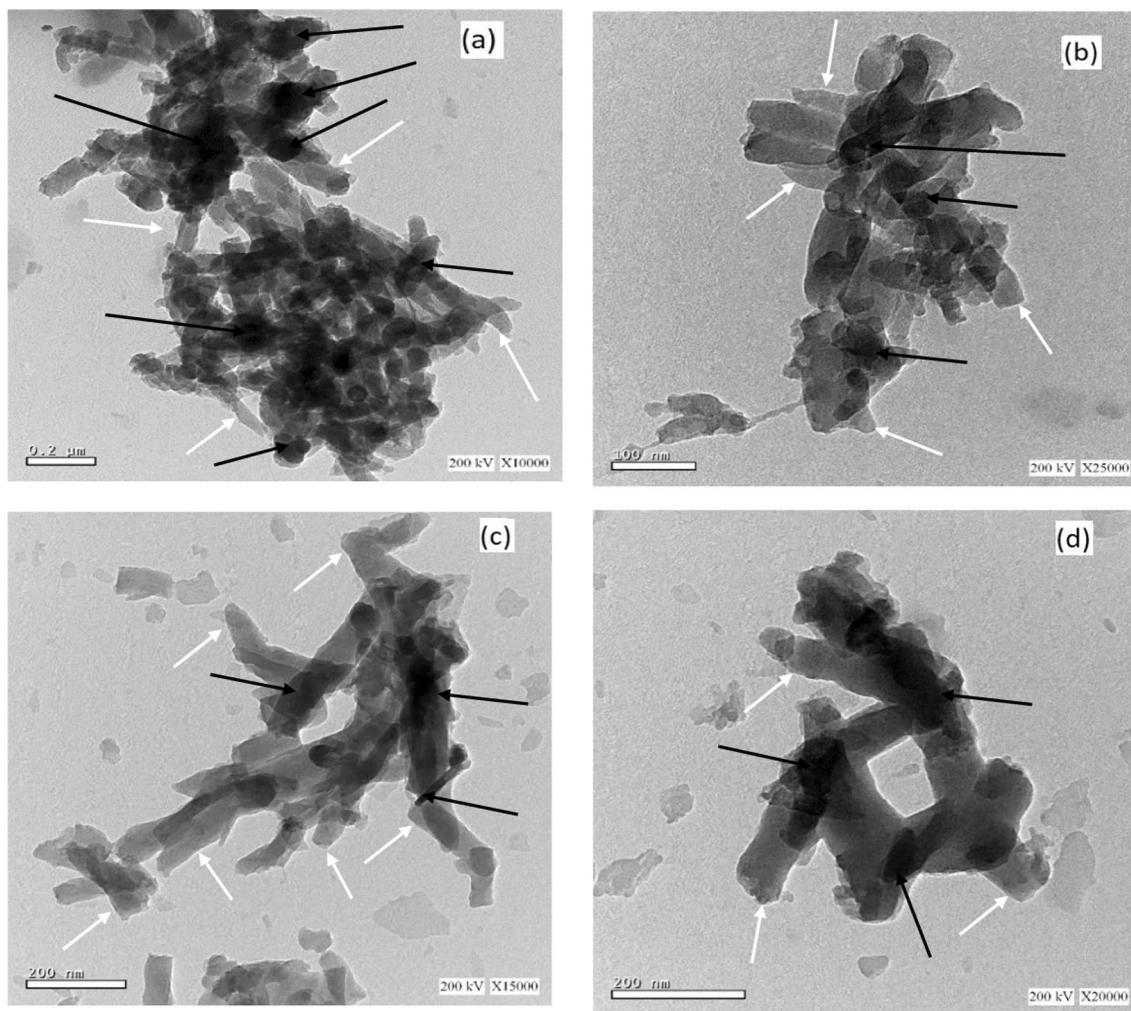


Fig. 11 HR-TEM micrographs of PANI nanocomposites loaded with Co-doped ZnO samples; **a, b** PANI-CZ1, **c, d** PANI-CZ5

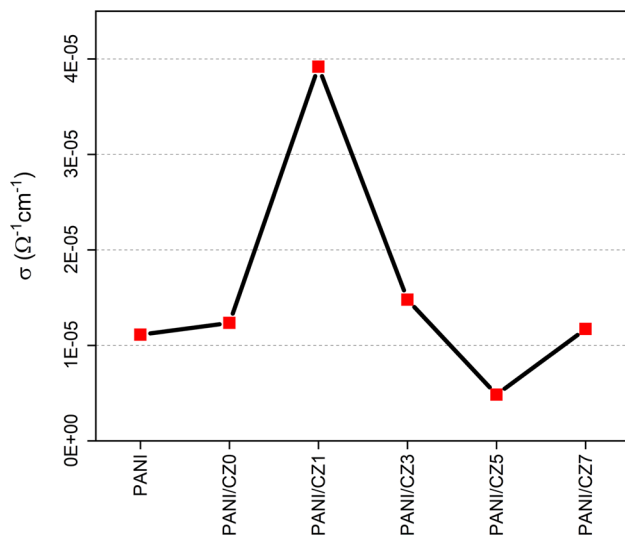


Fig. 12 Electrical conductivity (DC) for synthesized nanocomposites using 4-probe method at room temperature

Co-doped ZnO, usually has ferromagnetic behavior that is could be reflected on the degree of agglomeration of the used filler (Farha et al. 2016; Mansour et al. 2021). Indeed, there are many considerations which could be affected on the DC conductivity of the CP nanocomposites. Some of these considerations lead to the decrease in σ value such as: (i) the increase in the electronic scattering due to the good dispersion of nanoparticles throughout polymer matrix (Mansour et al. 2021) and (ii) the probable interruption of the chains ordering of polymer with the introduction of Co-doped ZnO (Mostafaei and Zolriasatein 2012; Kim and O'Shaughnessy 2003; Sharma et al. 2009). However, other considerations lead to the increase in σ value as a result of the improvement in the molecular ordering of the polymer due to the grown of polymer in the nanoscopically confined sites of the nanofiller (Cho et al. 2001).

Photocatalytic oxidation study

Effect of different photocatalysts

To investigate the best cobalt doping percentage added to maximize the catalytic activity of the prepared samples (PANI/CZ), various catalysts with various percentages were checked on Procion Blue (MX-7RX) oxidation. Figure 13 illustrates the plots of different catalyst behavior on the dye oxidation using 10 ppm Procion Blue at RT, 20 mg/L of the catalyst and keeping the pH of the wastewater at its original value. As seen from Fig. 12, PANI/CZ1 recorded the highest oxidation percentage that is reached to 93% within 90 min of irradiation time. This could be due to various reasons including: the small particle size, charge separation and large

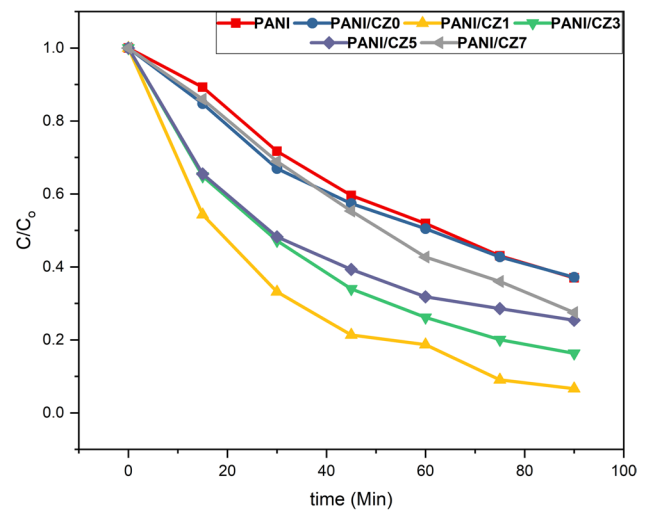


Fig. 13 Effect of different photocatalysts on photocatalytic oxidation for Procion Blue under UV light (photocatalyst dose = 20 mg L⁻¹, pH = 7, dye concentration = 10 ppm and room temperature)

content of oxygen vacancies or defects which is produced by doping with Co⁺² that reduces the recombination process (Xu et al. 2010). The main oxidizing species in the reaction media are the OH radicals. Such radicals generated in the reaction medium are non-selective. ·OH radicals attack the dye molecules and strongly oxidize them. Furthermore, the increase in the electrical conductivity since the increase in the electron-hole pairs helps in the generation of more radicals that helps in oxidizing more pollutant (Zhang et al. 2014). However, increasing the cobalt percentage covered the active surface of ZnO and thus reduces the dye oxidation (Adeel et al. 2021). Primarily, the PANI-CZ catalyst can promote the photocatalytic reaction across acyclic reaction. The displacement of a water molecule from the first solvation layer of the catalyst is suggested as the favorable process. OH radicals are signified as the main horsepower of oxidation reaction. When the initiation reaction is preceded under ultraviolet illumination, extra hydroxyl radicals are generated. The overall reaction is the produced radicals attacking the dye molecules to further intermediate and harmless end products (Thabet et al. 2022a).

Moreover, to attain the optimum operating conditions, PANI/CZ1 was tested under different conditions to further maximize the oxidation performances. Hence, in this concept the catalyst concentration, operating temperature, pH and dye concentration are then checked.

Effect of photocatalyst dose

Various catalyst (PANI/CZ1) concentrations are investigated and the results are displayed in Fig. 14 using 10 ppm dye at RT and original pH of the aqueous dye solution. It is

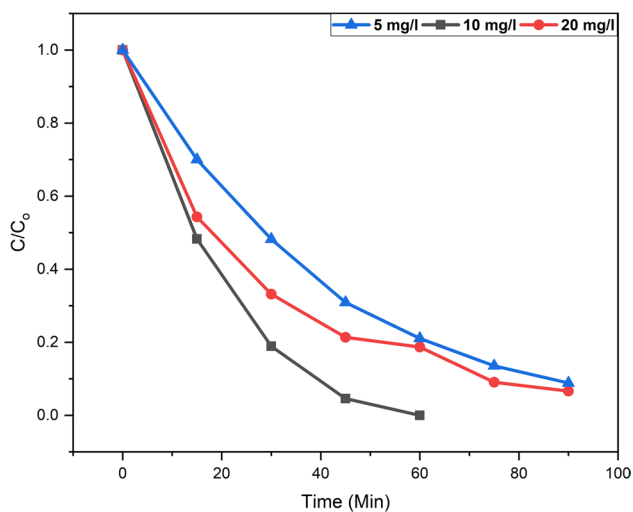


Fig. 14 Effect of the photocatalyst dose on the photo-oxidation of Procion Blue for PANI/CZ1 photocatalyst under UV illumination (photocatalyst dose = 10 mg L^{-1} , pH = 7 and dye concentration = 10 ppm)

revealed from the data in plot that reducing the catalyst concentration to 10 mg/L enhances the oxidation process and minimizing the oxidation time. Since the oxidation reaction takes place in only 60 min of illumination time with complete dye oxidation reached to 100% removal. However, 93% of dye oxidation is only attained in 90 min when 20 mg/L is applied to the oxidation reaction. To add up, as seen from the plot in Fig. 14, when 5 mg/L of PANI/CZ1 is subjected to the oxidation medium the reaction is hindered and only 91% of the dye is oxidized in 90 min of reaction time. This could be illustrated by the increase in the photocatalyst concentration over the optimal dose may lead to particles aggregation that takes place, which results in a significant reduction of electron–hole pairs and hence hinders the radicals' production (Yimer et al. 2014; Tju et al. 2017). However, when less catalyst is used it means the catalyst is insufficient to complete the oxidation reaction in the aqueous medium. This is in agreement with the previously cited in the literature by Tju et al. (2017) who reported that same catalytic dosage in methylene blue (MB) oxidation using $\text{ZnO/CeO}_2/\text{nanographene platelets}$ photocatalyst.

Effect of pH

Aqueous solutions' pH has a significant role on the rate of reaction taking place on semiconductor surfaces since its influences on surface charge properties of the photocatalysts (Yimer et al. 2014). Figure 15 displays the effect of pH change on dye oxidation (using 10 ppm dye; 10 mg/L PANI/CZ1 and at RT). As illustrated in Fig. 15, increasing the initial pH value greater than its original pH of the wastewater which recorded 7, nor decreasing such value, results in a

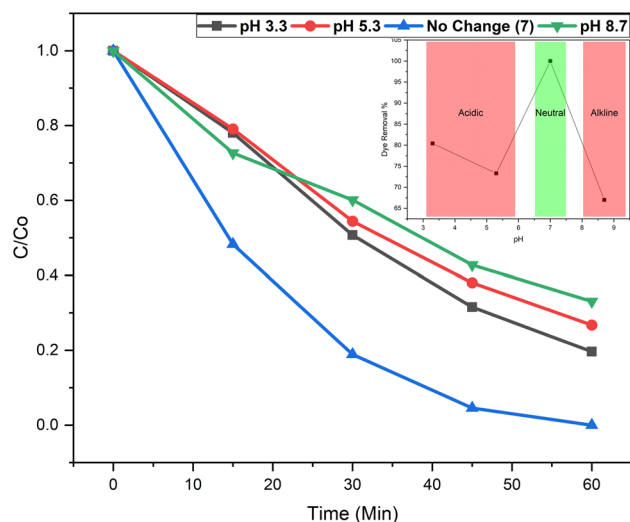


Fig. 15 effect of pH on the photo-oxidation of Procion Blue for PANI/CZ1 photocatalyst under UV illumination (photocatalyst dose = 10 mg L^{-1} , pH = 7 and dye concentration = 10 ppm)

reduction in the oxidation efficiency. It can be attributed to aggregation of charge on the outer of the synthesized nano-composites which significantly effect on their dispersion in dye solution (Abbasi and Hasanpour 2017). Also, it could be because less hydroxyl radicals are generated which is related to the optimal pH value (Tony and Mansour 2019). Although the photo-oxidation of PANI/CZ1 in acidic solution (3.3 and 5.3) is better than that in the alkaline solution (8.7), the best oxidation results are attained at the neutral pH conditions. This could be related to the reaction between organic compounds and dissolved oxygen is better at the neutral pH conditions. Moreover, the reaction of radical species generation, that are the main responsible of the reaction, is related to the pH of the medium (Abbasi and Hasanpour 2017). Abbasi et al. (2017) reported that the optimal pH value for photo-degradation efficiency of methylene orange, applied at different photocatalysts such as ZnO , SnO_2 and ZnO-SnO_2 , was pH = 7 rather than acidic (pH = 4) and alkaline (pH = 10) which confirm the obtained results in the present work.

Effect of Temperature

Changing the temperature of solution during oxidation process from RT to $60 \text{ }^\circ\text{C}$ was studied and illustrated in Fig. 16 (using 10 ppm of dye, 10 mg/L of PANI/CZ1 and pH 7). It is found that increasing solution temperature reduces dye removal efficiency as lower OH radicals are produced at the higher temperature values. Such radicals are considered the chief responsible of the oxidation reaction; therefore, the oxidation yield is deduced. The removal percentage reduces from 100% at room temperature to 23.5% at $60 \text{ }^\circ\text{C}$ in 60 min of illumination time.

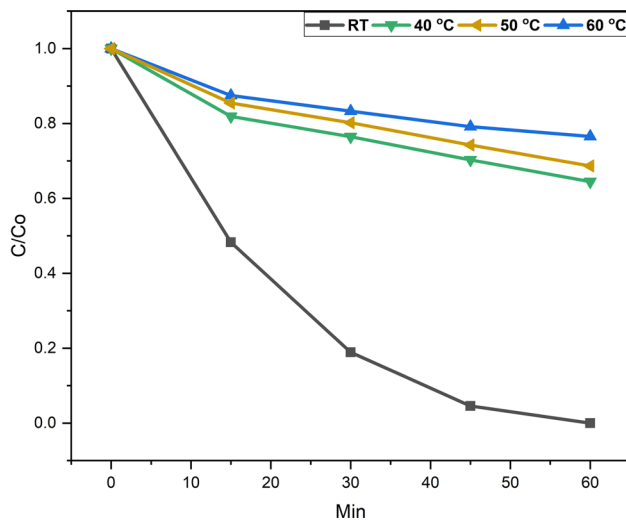


Fig. 16 Effect of Temperature on the photo-oxidation of Procion Blue for PANI/CZ1 photocatalyst under UV illumination (photocatalyst dose = 10 mg L⁻¹, pH = 7 and dye concentration = 10 ppm)

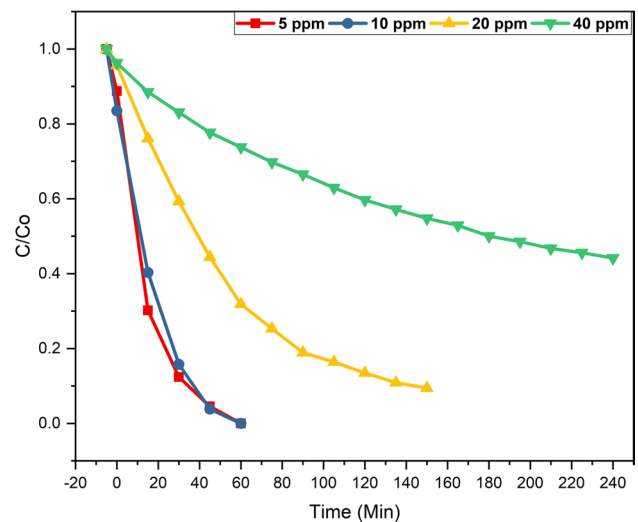


Fig. 17 Effect of initial dye concentration on the photo-oxidation of Procion Blue for PANI/CZ1 photocatalyst under UV illumination (photocatalyst dose = 10 mg L⁻¹, pH = 7 and room temperature)

This is in agreement with the previously reported by Barakat et al. (2013) who applied Ag-doped TiO₂ nanofibers for the photo-oxidation of Rhodamine B dye under UV illumination and they concluded that increasing temperature over 25 °C showed a negative effect on the dye oxidation. However, different results were reported for treating such dye using other catalyst since they reported that increasing the temperature to 60 °C slightly increases the MX-7RX dye removal rate using photo-Fenton system (Tony and Mansour 2019). Here, it is worth to mention that the obtained adverse effect of the temperature on the photo-degradation process of pollutants could be clarified in view of the surface energy feature of the used photocatalysts (Prousek 1996). More specifically, the surface to volume ratio of 1D nanostructure such as nanorods (as in case of the present study) is higher than that ratio for 3D nanostructure as nanospheres. The high surface area of the particles enables to obtain a high surface energy of such particles that could be activated the photocatalysis reaction as expected at normal ambient condition for 1D shape. By increasing the temperature, the surface energy of the photocatalysts increases and may be reached to ultra-active surface which leads to escaping the pollutant molecules from the active zones surrounding the nanorods that lead to a decrease in the photocatalytic activity. Although temperature has an adverse effect on the 1D nanostructure shape, charge carrier transfer at low temperatures is more promoted in comparison with the 3D shape due to the large surface-to-volume ratio in the case of 1D, resulting in high freedom for charge carriers. That plays a crucial role in the oxidation process of organic dyes.

Effect of initial dye loading

For the object of real applications, various dye concentrations including higher doses were checked to investigate the system reality. The effect of changing the dye concentration, from 5 to 40 ppm, on the oxidation activity at RT and 10 mg/L of catalyst concentration at normal pH of wastewater is displayed in Fig. 17. The highest oxidation rate was recorded at the low dye concentrations (5 and 10 ppm). This is because the small amount of dye concentration is oxidized at the same amount of the photocatalyst which is kept constant. However, while increasing the dye concentration, at the same catalyst dose, the radicals generated are insufficient to oxidize the amount of the dye molecules and the oxidation yield is reduced (Yimer et al. 2014). Also, increasing the dye concentration could cause shadowing effect which prevents the UV radiation from penetrating the solution and thus low radicals yield is generated in the reaction medium and the oxidation is hindered (Tony and Mansour 2019).

Oxidation kinetics

To fully understand the oxidation of PANI/CZ1 on the dye oxidation, the oxidation kinetics was studied at various initial dye concentrations ranging from 5 to 40 ppm. Zero-, first- and second-order kinetics were estimated, by calculating the slope of linear plot of concentration (C) vs. time (t), $\ln(C)$ vs. t and $1/(C)$ vs. t for zero-, first- and second-order reaction, respectively, and plotted according to the linearized equations form of the models (plots are not included). Then, slopes and intercepts of these plots are used to determine the reaction kinetic constants (K_0 , K_1 and K_2) and half-life time

($t_{1/2}$), which are listed in Table 3 as well as the regression coefficients (R^2) that were used to evaluate such models. Based on (R^2) values listed on Table 3, first-order reaction system possesses the highest values for all dye concentrations 5, 10, 20 ppm systems compared to zero- or second-order systems. In only 40 ppm system, the second order had higher R^2 value than first order with small value. Hence, the Procion Blue photocatalysis oxidation followed first-order kinetic reaction. Tony and Mansour (2019) reported that the Procion Blue followed second-order kinetic reaction using Fe_2O_3 photo-Fenton system while changing system temperature up to 60 °C.

Table 4 tabulates a comparison between current study and other previous studies reported in the literature for various organic dyes removals from aqueous solution by oxidation treatment. It is observed that current study, PANI/CZ1, could show a complete removal of Procion Blue commercial dye in 30 min, reaction time, using low photocatalyst concentration compared to other listed in Table 4. It can be concluded from the table that although a high removal efficiency is achieved, they have some disadvantage such as high photocatalyst dose (Mitra et al. 2017; Olad and Nosrati 2012; Ahmad et al. 2013; Gaim et al. 2019; Kumar 2018), pH adjustment (Tony and Mansour 2019, 2020b), presence of hydrogen peroxide (H_2O_2) (Tony and Mansour 2019, 2020b) and/or temperature treatment (Tony and Mansour 2019, 2020b) which gain the benefit of no further treatment that is required for current study. Moreover, comparing current dye removal process with photo-Fenton process (Tony and Mansour 2019, 2020b) listed in Table 4, Fenton process produces iron sludges that need to be removed after treatment, the pH required to be adjusted to the acidic region (pH 3) and after oxidation process the wastewater required neutralization of pH (Domingues et al. 2018).

Conclusion

Co-doped ZnO nanorods have been synthesized via hydrothermal route. The microstructural and morphological results confirmed the formation of high quality of such nanorods with replacement of Zn ions by Co ions in the ZnO host matrix. Moreover, the obtained UV-Vis absorbance results definite the blue shift band gaps of the investigated nanorods with Co content increasing. PANI/Co-doped ZnO NCs were successfully fabricated using in situ oxidative polymerization. The obtained microstructural and morphological results showed quite good interaction between nanorod fillers and PANI matrix. Moreover, the values of DC conductivity show high slightly increase for the nanocomposites with Co-doped ZnO nanorods compared with the undoped PANI. Subsequently, the photocatalytic activity of PANI/Co-doped ZnO nanocomposites, as new photocatalyst, for Procion Blue dye remediation was studied and the optimum operating parameters were monitored. A complete dye removal was attained within 60 min of irradiance time using 10 mg/L, PANI-CZ1 photocatalyst at pH 7.0 and RT. The kinetics of the oxidation was studied, and the reaction is following the first-order reaction rate. To conclude, the obtained data confirmed the importance of nanostructured fillers in improving the conductive polymers' performance that is appeared in the enhancement of the electrical conductivity and photocatalytic activity of the investigated nanocomposites. Also, the used facile fabrication route of PANI/Co-doped ZnO nanocomposites and the obtained results are encouraging the usage of polyaniline nanocomposites based on wide band-gap metal oxide nanoparticles in the field of wastewater treatment.

Table 3 Zero-, first- and second-order kinetic rate constants (K_0 , K_1 and K_2) and reaction half-life ($t_{1/2}$) of Procion Blue photocatalytic oxidation at different concentrations

Dye concentration (ppm)	Zero-order reaction Rate : $-\frac{d[C]}{dt} = K$		First-order reaction Rate : $-\frac{d[C]}{dt} = K[C]$		Second-order reaction Rate : $-\frac{d[C]}{dt} = K[C]^2$				
	$K_0 \times 10^{-2} (\text{mg l}^{-1} \text{min}^{-1})$	R^2	$t_{1/2} (\text{min})^*$	$K_1 \times 10^{-2} (\text{min}^{-1})$	R^2	$t_{1/2} (\text{min})^{**}$	$K_2 \times 10^{-2} (\text{mg}^{-1} \text{min}^{-1})$	R^2	$t_{1/2} (\text{min})^{***}$
5	1.803	0.84	20.67	6.547	1	10.59	38.421	0.92	3.06
10	1.756	0.93	21.46	6.792	0.98	10.21	42.164	0.84	2.79
20	0.544	0.87	71.08	1.596	0.99	43.43	5.537	0.98	21.25
40	0.205	0.95	214.70	0.319	0.99	217.29	0.635	1	185.27

* $t(1/2) = [C]_0/2K$; ** $t(1/2) = \ln(2)/K$; *** $t(1/2) = 1/K[C]_0$

Table 4 Comparison of various organic dyes removals in aqueous media using different oxidation treatment systems

Catalyst	Catalyst dose (mg/L)	pH	Preparation method	Dye (concentration, ppm)	UV source	Radiation time (min)	Dye removal (%)	Ref
PANI/CZ1 photocatalyst	10	7	In situ PANI oxidative polymerization in the presence of cobalt-doped zinc oxide by hydrothermal route	Procion Blue (10)	Artificial UV	60	100	Current study
Fe ₂ O ₃ Photo-Fenton system	Catalyst = 40 H ₂ O ₂ = 800	2.8	Simple sol–gel route using FeCl ₃	Procion Blue (38)	Artificial UV	60	76.0	Tony and Mansour (2019)
Fe ₃ O ₄ Photo-Fenton system	Catalyst = 48 H ₂ O ₂ = 828		Co-precipitation route	Levafix Blue dye (20)	Artificial UV	30	99	Thabet et al. (2023)
PANI-ZnO photocatalyst	1500	NA	In situ chemical polymerization	Methylene Blue (10)	Visible light	60	82.0	Olad and Nosrati (2012)
PANI/Al-ZnO photocatalyst	400	7	In situ PANI oxidative polymerization in the presence of cobalt-doped zinc oxide by hydrothermal route	Methylene orange (3.3)	Visible light	150	92.5	Mitra et al. (2017)
PANI/Al-ZnO photocatalyst	400	7	In situ PANI oxidative polymerization in the presence of cobalt-doped zinc oxide by hydrothermal route	Rose Bengal (9.7)	Visible light	150	98.0	Mitra et al. (2017)
Magnetite photocatalyst	Catalyst = 80 H ₂ O ₂ = 1600		Simple co-precipitation	Methylene blue (10)	Artificial UV	180	94%	Thabet et al. (2020)
Cu-doped ZnO/Carbon nanotubes (CNTs) photocatalyst	1000	NA	Facile sol method	Methylene Orange (20)	Visible light	120	98.21	Ahmad et al. (2013)
Aluminum/magnetite	Catalyst = 1000 H ₂ O ₂ = 800		Hydrothermal technique	Levafix Blue CA (20)	Artificial UV		99	Thabet et al. (2022b)
TiO ₂ /PANI photocatalyst	800	7	Oxidation polymerization method	Rose Bengal (6.25)	Visible light	120 min	93.0	Kumar (2018)
TiO ₂ /PANI/GO photocatalyst	800	7	Oxidation polymerization method	Rose Bengal (6.25)	Visible light	120 min	97.0	Kumar (2018)
N-doped Cu ₂ O/ZnO photocatalyst	180	NA	Co-precipitation and thermal decomposition methods	Methyl Red (40)	Solar light	180 min	93.5	Gaim et al. (2019)
Fe ₂ O ₃ Hematite nanocrystals	Catalyst = 40 H ₂ O ₂ = 400	3	Simple sol–gel	Bismarck dye (33.8)	Solar light	60	92.0	Tony et al. (2020)

Table 4 (continued)

Catalyst	Catalyst dose (mg/L)	pH	Preparation method	Dye (concentration, ppm)	UV source	Radiation time (min)	Dye removal (%)	Ref
Fe ₂ O ₃ Hematite nanocrystals	Catalyst = 40 H ₂ O ₂ = 400	3	Simple sol-gel	Bismarck dye (5)	Solar light	60	59.0	Tony et al. (2020)

PANI polyaniline, NA not applicable, UV ultraviolet

Funding Open access funding provided by The Science, Technology & Innovation Funding Authority (STDF) in cooperation with The Egyptian Knowledge Bank (EKB). The author(s) received no specific funding for this work.

Declarations

Conflict of interest The authors confirm that there is no conflict of interest.

Open Access This article is licensed under a Creative Commons Attribution 4.0 International License, which permits use, sharing, adaptation, distribution and reproduction in any medium or format, as long as you give appropriate credit to the original author(s) and the source, provide a link to the Creative Commons licence, and indicate if changes were made. The images or other third party material in this article are included in the article's Creative Commons licence, unless indicated otherwise in a credit line to the material. If material is not included in the article's Creative Commons licence and your intended use is not permitted by statutory regulation or exceeds the permitted use, you will need to obtain permission directly from the copyright holder. To view a copy of this licence, visit <http://creativecommons.org/licenses/by/4.0/>.

References

- Abbasi S, Hasanpour M (2017) The effect of pH on the photocatalytic degradation of methyl orange using decorated ZnO nanoparticles with SnO₂ nanoparticles. *J Mater Sci: Mater Electron* 28:1307–1314
- Adeel M, Saeed M, Khan I, Muneer M, Akram N (2021) Synthesis and characterization of Co-ZnO and evaluation of its photocatalytic activity for photodegradation of methyl orange. *ACS Omega* 6:1426–1435
- Ahmad M, Ahmed E, Hong ZL, Jiao XL, Abbas T, Khalid NR (2013) Enhancement in visible light-responsive photocatalytic activity by embedding Cu-doped ZnO nanoparticles on multi-walled carbon nanotubes. *Appl Surf Sci* 285:702–712
- Barakat NAM, Kanjwal MA, Chronakis IS, Kim HY (2013) Influence of temperature on the photodegradation process using Ag-doped TiO₂ nanostructures: negative impact with the nanofibers. *J Mol Catal a: Chem* 366:333–340
- Bazin I, Hassine AIH, Hamouda YH, Mnif W, Bartegi A, Lopez-Ferber M, Waard MD, Gonzalez C (2012) Estrogenic and anti-estrogenic activity of 23 commercial textile dyes. *Ecotoxicol Environ Saf* 85:131–136
- Chatterjee SK (2008) Crystallography and the world of symmetry, vol 113. Springer, Berlin
- Chen Z, Li Y, Cai Y, Wang S, Hu B, Li B, Ding X, Wang X (2023) Application of covalent organic frameworks and metal-organic frameworks nanomaterials in organic/inorganic pollutants removal from solutions through sorption-catalysis strategies. *Carbon Res*. <https://doi.org/10.1007/s44246-023-00041-9>
- Cheng B, Samulski ET (2004) Hydrothermal synthesis of one-dimensional ZnO nanostructures with different aspect ratios. *Chem Commun* 8:986–986
- Cho G, Fung BM, Glatzhofer DT, Lee J-S, Shul Y-G (2001) Preparation and characterization of polypyrrole-coated nanosized novel ceramics. *Langmuir* 17:456–461
- Cia Y, Chen Z, Wang S, Chen J, Hu B, Chen C, Wang X (2023) Carbon-based nanocomposites for the elimination of inorganic and organic pollutants through sorption and catalysis strategies. *Sep Purif Technol* 308:122862. <https://doi.org/10.1016/j.seppur.2022.122862>
- Domingues E, Gomes J, Quina M, Quinta-Ferreira R, Martins R (2018) Detoxification of Olive Mill Wastewaters by Fenton's Process. *Catalysts* 8:662
- Epolito W, Lee Y, Bottomley L, Pavlostathis S (2005) Characterization of the textile anthraquinone dye Reactive Blue 4. *Dyes Pigm* 67:35–46
- Farha AH, Mansour SA, Kotkata MF (2016) Structural, optical, and magnetic study of dilute magnetic semiconducting Co-doped ZnO nanocrystals synthesized using polymer-pyrolysis route. *J Mater Sci* 51:9855–9864
- Gaim YT, Tesfamariam GM, Nigussie GY, Ashebir ME (2019) Synthesis, characterization and photocatalytic activity of N-doped Cu₂O/ZnO nanocomposite on degradation of methyl red. *J Compos Sci* 3:93
- Hammad TM, Salem JK, Harrison RG (2012) Structure, optical properties and synthesis of Co-doped ZnO superstructures. *Appl Nanosci* 3:133–139
- Hammad TM, Salem JK, Harrison RG (2013) Structure, optical properties and synthesis of Co-doped ZnO superstructures. *Appl Nanosci* 3:133–139
- Kaphle A, Reed T, Apblett A, Hari P (2019) Doping efficiency in cobalt-doped ZnO nanostructured materials. *J Nanomater*. <https://doi.org/10.1155/2019/7034620>
- Kim J, O'Shaughnessy B (2003) Morphology selection of nanoparticle dispersions by polymer media. *Phys Rev Lett* 89:238301
- Kositzi M, Poullos I, Malato S, Caceres J, Campos A (2004) Solar photocatalytic treatment of synthetic municipal wastewater. *Water Res* 38:1147–1154
- Kumar A (2018) Comparative photocatalytic degradation of rose Bengal Dye under visible light by TiO₂, TiO₂/PANI and TiO₂/PANI/GO nanocomposites. *Int J Res Appl Sci Eng Technol* 6:339–350
- Kumbhakar P, Singh D, Tiwary CS, Mitra AK (2008) Chemical synthesis and visible photoluminescence emission from monodispersed ZnO nanoparticles. *Chalcogenide Lett* 5:387–394
- Langford JI, Wilson AJC (1978) Scherrer after sixty years: a survey and some new results in the determination of crystallite size. *J Appl Crystallogr* 11:102–113

- Lellis B, Fávoro-Polonio CZ, Pamphile JA, Polonio JC (2019) Effects of textile dyes on health and the environment and bioremediation potential of living organisms. *Biotechnol Res Innov* 3:275–290
- Liu X, Li Y, Chen Z, Yang H, Wang S, Chen J, Hu B, Huang Q, Shen C, Wang X (2023) Advanced porous nanomaterials as superior adsorbents for environmental pollutants removal from aqueous solutions. *Crit Rev Environ Sci Technol* 53(13):1289. <https://doi.org/10.1080/10643389.2023.2168473>
- Mansour S, Farha A, Kotkata M (2017) Synthesis and study of ZnO nanoparticles by polymer pyrolysis route using two different polymerization initiators. *Int J Appl Ceram Technol* 14:1213–1221
- Mansour SA, Farha AH, Tahoun BA, Elsad RA (2021) Novel magnetic polyaniline nanocomposites based on as-synthesized and surface modified Co-doped ZnO diluted magnetic oxide (DMO) nanoparticles. *Mater Sci Eng, B* 265:115032
- Mesaros A, Ghitulica CD, Popa M, Mereu R, Popa A, Petrisor T Jr, Gabor M, Cadis AI, Vasile BS (2014a) Synthesis, structural and morphological characteristics, magnetic and optical properties of Co doped ZnO nanoparticles. *Ceram Int* 40:2835–2846
- Mitra M, Ghosh A, Mondal A, Kargupta K, Ganguly S, Banerjee D (2017) Facile synthesis of aluminium doped zinc oxide-polyaniline hybrids for photoluminescence and enhanced visible-light assisted photo-degradation of organic contaminants. *Appl Surf Sci* 402:418–428
- Mostafaei A, Zolriasatein A (2012) Synthesis and characterization of conducting polyaniline nanocomposites containing ZnO nanorods. *Progr Nat Sci: Mater Int* 22:273–280
- Muralikrishna IV, Manickam V (eds) (2017) Principles and design of water treatment. In: Environmental management. Elsevier, Amsterdam, pp 209–248
- Neto NFA, Matsui KN, Paskocimas CA, Bomio MRD, Motta FV (2019) Study of the photocatalysis and increase of antimicrobial properties of Fe³⁺ and Pb²⁺ co-doped ZnO nanoparticles obtained by microwave-assisted hydrothermal method. *Mater Sci Semicond Process* 93:123–133
- Nirmala M, Anukaliani A (2011) Characterization of undoped and Co doped ZnO nanoparticles synthesized by DC thermal plasma method. *Physica B* 406:911–915
- Ocakoglu K, Mansour SA, Yildirimcan S, Al-Ghamdi AA, El-Tantawy F, Yakuphanoglu F (2015) Microwave-assisted hydrothermal synthesis and characterization of ZnO nanorods. *Spectrochim Acta Part A Mol Biomol Spectrosc* 148:362–368
- Olad A, Nosrati R (2012) Preparation, characterization, and photocatalytic activity of polyaniline/ZnO nanocomposite. *Res Chem Intermed* 38:323–336
- Ozgiir U, Alivov YI, Liu C, Teke A, Reshchikov MA, Dogan S, Avrutin V, Cho SJ, Morkoc H (2005) A comprehensive review of ZnO materials and devices. *J Appl Phys* 98:041301
- Patterson AL (1939) The Scherrer Formula for X-ray particle size determination. *Phys Rev* 56:978–982
- Pirsaheb M, Moradi S, Shahlaei M, Wang X, Farhadian N (2019) A new composite of nano zero-valent iron encapsulated in carbon dots for oxidative removal of bio-refractory antibiotics from water. *J Clean Prod* 209:1523–1532
- Pouget JP, Jozefowicz ME, Epstein AJ, Tang X, MacDiarmid AG (1991) X-ray structure of polyaniline. *Macromolecules* 24:779–789
- Prousek J (1996) Advanced oxidation processes for water treatment. Chemical process. *Chem Listy* 90:229–237
- Sakai K, Kakeno T, Ikari T, Shirakata S, Sakemi T, Awai K, Yamamoto T (2006) Defect centers and optical absorption edge of degenerated semiconductor ZnO thin films grown by a reactive plasma deposition by means of piezoelectric photothermal spectroscopy. *J Appl Phys* 99:043508–043508
- Scherrer P (1918) Bestimmung der Größe und der inneren Struktur von Kolloidteilchen mittels Röntgenstrahlen. *Nachrichten Von Der Gesellschaft Der Wissenschaften Zu Gottingen, Mathematisch-Physikalische Klasse* 1918:98–100
- Schroder DK, Corporation E (2006) Semiconductor Material and Device Characterization. Wiley
- Senthilkumar V, Vickraman P, Jayachandran M, Sanjeeviraja C (2010) Structural and electrical studies of nano structured Sn_{1-x}Sb_xO₂ (x = 0.0, 1, 2.5, 4.5 and 7 at%) prepared by co-precipitation method. *J Mater Sci: Mater Electron* 21:343–348
- Sharma BK, Khare N, Dhawan SK, Gupta HC (2009) Dielectric properties of nano ZnO-polyaniline composite in the microwave frequency range. *J Alloys Compd* 477:370–373
- Sharma S, Singh S, Khare N (2016) Synthesis of polyaniline/CdS (nanoflowers and nanorods) nanocomposites: a comparative study towards enhanced photocatalytic activity for degradation of organic dye. *Colloid Polym Sci* 294:917–926
- Shi L, Wang X, Lu L, Yang X, Wu X (2009) Preparation of TiO₂/polyaniline nanocomposite from a lyotropic liquid crystalline solution. *Synth Met* 159:2525–2529
- Shi S, Yang Y, Xu J, Li L, Zhang X, Hu G-H, Dang Z-M (2013) Structural, optical and magnetic properties of Co-doped ZnO nanorods prepared by hydrothermal method. *J Alloys Compd* 576:59–65
- Thabet R, Tony M, El Sherbiney S, Ali IA, Fouad M (2020) Catalytic oxidation over nanostructured heterogeneous process as an effective tool for environmental remediation. *IOP Conf Ser: Mater Sci Eng* 975:012004
- Thabet RH, Fouad MK, Ali IA, El Sherbiney SA, Tony MA (2021) (2021) Magnetite-based nanoparticles as an efficient hybrid heterogeneous adsorption/oxidation process for reactive textile dye removal from wastewater matrix. *Int J Environ Anal Chem.* <https://doi.org/10.1080/03067319.2021.1896716>
- Thabet R, Fouad M, El Sherbiney S, Tony M (2022a) Construction of a hetero-junction recyclable composite photocatalyst from aluminum-based waste/magnetite for efficient carbamate insecticide oxidation. *Environ Sci: Water Res Technol* 8:1874
- Thabet R, Fouad M, El Sherbiney S, Tony M (2022b) Zero-waste approach: assessment of aluminum-based waste as a photocatalyst for industrial wastewater treatment ecology. *Int J Environ Res* 16(3):36. <https://doi.org/10.1007/s41742-022-00414-9>
- Thabet R, Fouad M, Ali IA, El Sherbiney S, Tony M (2023) Magnetite-based nanoparticles as an efficient hybrid heterogeneous adsorption/oxidation process for reactive textile dye removal from wastewater matrix. *Int J Environ Anal Chem* 103(11):2636–2658
- Tju H, Shabrany H, Taufik A, Saleh R (2017) Degradation of methylene blue (MB) using ZnO/CeO₂/nanographene platelets (NGP) photocatalyst: effect of various concentration of NGP. *AIP Conf Proc* 1862:030037
- Tony MA (2020) Central composite design optimization of Bismarck Dye oxidation from textile effluent with Fenton's reagent. *Appl Water Sci* 10:1–9
- Tony MA, Ali IA (2022) Mechanistic implications of redox cycles solar reactions of recyclable layered double hydroxides nanoparticles for remazol brilliant abatement. *Int J Environ Sci Technol* 19:9843–9860
- Tony MA, Mansour SA (2019) Removal of the commercial reactive dye Procion Blue MX-7RX from real textile wastewater using the synthesized Fe₂O₃ nanoparticles at different particle sizes as a source of Fentons reagent. *Nanoscale Adv* 1:1362–1371
- Tony MA, Mansour SA (2020a) Synthesis of nanosized amorphous and nanocrystalline TiO₂ for photochemical oxidation of methomyl insecticide in aqueous media. *Water Environ J* 34:239–249
- Tony M, Mansour SA (2020b) Microwave-assisted catalytic oxidation of methomyl pesticide by Cu/Cu₂O/CuO hybrid nanoparticles as a Fenton-like source. *Int J Environ Sci Technol* 17(1):161–174

- Tony MA, Mansour SA (2020c) Solar photo-Fenton reagent with nano-structured iron oxide for Bismarck dye oxidation: an Egyptian apparel case study. *Int J Environ Sci Technol* 17:1337–1350
- Tony MA, Mansour SA, Tayeb AM (2018) Purcell PJ (2018) PUse of a fenton-like process based on nano-haematite to treat synthetic wastewater contaminated by phenol: Process investigation and statistical optimization. *Arab J Sci Eng* 43:2227–2235
- Varghese PI, Pradeep T (2003) A textbook of nanoscience and nanotechnology. Tata McGraw-Hill Education, New York
- Wang S, Chen Z, Cai Y, Wu L, Wang S, Tang Z, Hu B, Li Z, Wang X (2023) Application of COFs in capture/conversion of CO₂ and elimination of organic/inorganic pollutants. *Environ Funct Mater*. <https://doi.org/10.1016/j.efmat.2023.03.001>
- Williamson GK, Hall WH (1953) X-ray line broadening from filed aluminium and wolfram. *Acta Metall* 1:22–31
- Xia H, Wang Q (2002) Ultrasonic irradiation: a novel approach to prepare conductive polyaniline/nanocrystalline titanium oxide composites. *Chem Mater* 14:2158–2165
- Xu C, Cao L, Su G, Liu W, Qu X, Yu Y (2010) Preparation, characterization and photocatalytic activity of Co-doped ZnO powders. *J Alloys Compd* 497:373–376
- Yahya SA, Musa IE, Amjad HE, Gavin MW (2008) Effect of solution pH, ionic strength, and temperature on adsorption behavior of reactive dyes on activated carbon. *Dyes Pigm* 77:16–23
- Yimer W, Yadav O, Kebede T (2014) Photo-catalytic removal of methyl orange dye by polyaniline modified ZnO using visible radiation. *Sci Technol Arts Res J* 3:93
- Yu JC, Yu J, Ho W, Jiang Z, Zhang L (2002) Effects of F-doping on the photocatalytic activity and microstructures of nanocrystalline TiO₂ powders. *Chem Mater* 14:3808–3816
- Zamani N, Modarresi-Alam AR, Noroozifar M, Javanbakht M (2019) The improved performance of lithium-ion batteries via the novel electron transport catalytic role of polyaniline (PANI) in PANI/Co 3 O 4–CuO raspberry as new anode material. *J Appl Electrochem* 49:327–340
- Zhang P, Hong RY, Chen Q, Feng WG (2014) On the electrical conductivity and photocatalytic activity of aluminum-doped zinc oxide. *Powder Technol* 253:360–367

Publisher's Note Springer Nature remains neutral with regard to jurisdictional claims in published maps and institutional affiliations.